Local Geometric and Transport Properties of Networks that are Generated from Hyperuniform Point Patterns

James V. Raj[1,*], Xiaohan Sun[2], Charles Emmett Maher[3], Katherine A. Newhall[3], and Mason A. Porter[2,4,5]

[1]*Department of Physics and Astronomy, University of California, Los Angeles, Los Angeles, CA, USA*
[2]*Department of Mathematics, University of California, Los Angeles, Los Angeles, CA, USA*
[3]*Department of Mathematics, University of North Carolina at Chapel Hill, Chapel Hill, NC, USA*
[4]*Department of Sociology, University of California, Los Angeles, Los Angeles, CA, USA and*
[5]*Santa Fe Institute, Santa Fe, NM, USA**

(Dated: November 25, 2025)

Hyperuniformity, which is a type of long-range order that is characterized by the suppression of long-range density fluctuations in comparison to the fluctuations in standard disordered systems, has emerged as a powerful concept to aid in the understanding of diverse natural and engineered phenomena. In the present paper, we harness hyperuniform point patterns to generate a class of disordered, spatially embedded networks that are distinct from both perfectly ordered lattices and uniformly random geometric graphs. We refer to these networks as *hyperuniform-point-pattern-induced (HuPPI) networks*, and we compare them to their counterpart *Poisson-point-pattern-induced (PoPPI) networks*. By computing the local geometric and transport properties of HuPPI networks, we demonstrate how hyperuniformity imparts advantages in both transport efficiency and robustness. Specifically, we show that HuPPI networks have systematically smaller total effective resistances, slightly faster random-walk mixing times, and fewer extreme-curvature edges than PoPPI networks. Counterintuitively, we also find that HuPPI networks simultaneously have more negative mean Ollivier–Ricci curvatures and smaller global resistances than PoPPI networks, indicating that edges with moderately negative curvatures need not create severe bottlenecks to transport. Moreover, HuPPI networks are consistently more robust under both random edge removals and curvature-based targeted edge removals, maintaining larger connected components for larger fractions of removed edges than their PoPPI counterparts. We also demonstrate that the network-generation method strongly influences these properties and in particular that it often overshadows differences that arise from underlying point patterns. These results collectively demonstrate potential advantages of hyperuniformity in network design and motivate further theoretical and experimental exploration of HuPPI networks.

I. INTRODUCTION

Networks arise in a wide variety of natural and engineered systems [1], and spatial embeddings and constraints play an essential role in many of these systems [2]. Because disordered systems offer a much larger design space than ordered systems, enabling greater tunability of transport and mechanical properties, recent work on spatially embedded network metamaterials has begun to exploit this flexibility [3].

From transportation infrastructure [4] and power grids [5] to neuronal networks [6] and protein-interaction networks [7, 8], spatial constraints play a fundamental role in shaping network structure and function. The geometric arrangement of nodes and the associated distances between them often constrain connectivity (e.g., by influencing measures like spatial strength centrality [9]), transport, and robustness [10]. Accordingly, there is considerable interest in understanding how different spatial point patterns, which range from uniformly random arrangements to highly correlated patterns, affect network properties after one uses such patterns to generate a network [2]. Indeed, the analysis of geometric networks that arise from point patterns is an important topic in the field of stochastic geometry [11]. One way to analyze the properties of such networks is through geometric data analysis and the examination of discrete curvature on networks [12]. Notions of network curvature have useful physical interpretations. For example, Devriendt et al. [13, 14] introduced a resistance-based notion of graph curvature that links effective resistance, commute times, and mixing behavior in networks. In the present paper, we work with classical Ollivier–Ricci curvature (ORC) in spatially embedded graphs (i.e., networks), and we highlight the broader theme that curvature statistics are closely related to transport efficiency. We use ORC instead of Forman–Ricci curvature [15] (which is another popular type of network curvature) because the definition of ORC is based on optimal transport, which aligns with our focus on network transport properties like total effective resistance and random-walk mixing times.

In our paper, we study several properties of *hyperuniform-point-pattern-induced (HuPPI) networks*. A point pattern is called "hyperuniform" if its local density fluctuations are suppressed at large length scales in comparison to the fluctuations in a typical disordered system [16]. A growing body of work has demonstrated that hyperuniformity imparts desirable physical properties to both point patterns and two-phase media [17]. For example, Chen and Torquato [18] demonstrated that

certain types of disordered HuPPI networks can achieve almost optimal effective conductivity and elastic moduli, highlighting transport advantages that hyperuniformity confers to networked two-phase media.

Researchers have begun to explore how hyperuniformity manifests in spatially embedded networks [19–21]. One approach is to use hyperuniform or nonhyperuniform point patterns to determine the locations of the nodes of a graph and to then assign edges between nodes using some geometric construction (e.g., a Delaunay or Voronoi tessellation). Maher et al. [19] demonstrated that certain tessellation-based networks partially inherit hyperuniformity properties of the underlying point pattern. Newby et al. [20, 21] illustrated that Voronoi and Delaunay tessellations that are generated from hyperuniform point patterns have narrower distributions of cell areas and reduced local density correlations than networks that one constructs from Poisson-distributed points.

In the present paper, we investigate the properties that HuPPI networks inherit from the underlying hyperuniformity of their point patterns. Much is known about the transport properties of hyperuniform two-phase media [17, 22, 23], yet there is little understanding of the transport properties of HuPPI networks. Our aim is observational: we build HuPPI and Poisson-point-pattern-induced (PoPPI) networks and study whether and how the properties of the ensuing network families differ from each other.

Three lessons emerge. First, total effective resistances (TER) [24] and random-walk mixing times [25], which are global measures of transport in networks, are smaller in HuPPI networks than in PoPPI networks. This is consistent with findings on two-phase hyperuniform materials [18], where the specific microstructure geometry and topology are the primary determinants of effective transport properties. The method of network generation establishes a structure's fundamental topology (e.g., triangle-rich versus tree-like structures), which impacts baseline transport efficiency more strongly than the variations that arise due to underlying point patterns. However, the method of network generation (e.g., Delaunay tessellations, Voronoi tessellations, Delaunay-centroidal tessellations, or Gabriel graphs) [2, 18] has a much larger impact than the underlying point pattern on these global measures. Second, we observe that the differences that are consistent across network-generation methods are not driven directly by suppressed density fluctuations. Instead, they stem from the way that hyperuniformity biases local edge geometry, thereby narrowing the ORC distribution and reducing the frequency of extreme bottleneck edges. We compute ORC [26, 27], which is a discrete analogue of the Ricci curvature from geometry [28], to determine locally how "bottleneck-like" an edge is by comparing the optimal-transport cost that is required to transform the probability distribution of the neighborhood of one of its attached nodes into the probability distribution of the neighborhood of its other attached node. When the neighborhoods of two connected nodes

share many common neighbors, the optimal-transport cost is low (i.e., the associated curvature is positive), whereas a lone bridge-like edge has a high transport cost (i.e., an associated negative curvature) [26, 27]. Third, the TERs and random-walk mixing times of HuPPI networks are smaller in magnitude than those of PoPPI networks, despite often having more negative mean curvatures. This counterintuitive result arises because hyperuniformity suppresses extreme curvature outliers. PoPPI networks possess a few edges with large-magnitude negative curvatures that act as bottlenecks and inflate the TER. By contrast, HuPPI networks do not have many edges with large-magnitude negative curvatures and instead have many edges with small-magnitude negative curvatures, which do not create severe flow constraints.

Our paper proceeds as follows. In Sec. II, we review the idea of hyperuniformity and discuss the standard classification of different types of hyperuniformity. In Sec. III, we describe our procedures to generate HuPPI networks and PoPPI networks using Delaunay, Gabriel, Voronoi, and Delaunay-centroidal constructions. We also outline the methods that we use to compute ORCs, TERs, random-walk mixing times, and robustness in our networks. In Sec. IV, we compare the global transport properties of HuPPI networks and PoPPI networks. We demonstrate that HuPPI networks usually have smaller TERs and shorter random-walk mixing times than PoPPI networks. In Sec. V, we examine ORC statistics to explain these global differences at the level of edges. In Sec. VI, we evaluate network robustness under both random edge removal and curvature-based targeted edge removal, and we thereby highlight robustness advantages of HuPPI networks over PoPPI networks. Finally, in Sec. VII, we conclude and discuss the implications of our results for the design of spatially embedded networks. Our code to generate our networks, analyze our networks, and generate our figures is available at `https://github.com/DMREF-networks/HuPPI-Network-Analysis`.

II. HYPERUNIFORMITY

In this section, we define the notion of a hyperuniform point pattern in terms of number-variance scaling and present one method to generate such point patterns. Let $N(\Omega)$ be a random variable that indicates the number of points in a bounded spherical region $\Omega \subset \mathbb{R}^d$ of volume $|\Omega|$. The variance of the number of points is

$$\sigma_N^2(\Omega) = \left\langle N(\Omega)^2 \right\rangle - \left\langle N(\Omega) \right\rangle^2 . \tag{1}$$

A point pattern is *hyperuniform* [17] if the number variance satisfies

$$\lim_{R \to \infty} \frac{\sigma_N^2(\Omega_R)}{|\Omega_R|} = 0 , \tag{2}$$

where R is the radius (or any other linear measure of size) of a spherical observation window. That is, a point

pattern is hyperuniform if the number variance grows more slowly than the window's volume (e.g., slower than R^d if Ω_R is a ball of radius R).

One can subdivide hyperuniform point patterns into three classes based on the leading-order scaling of $\sigma_N^2(\Omega_R)$ in the $R \longrightarrow \infty$ (i.e., "large-R") regime [17, 29]:

1. Class I: $\sigma_N^2(\Omega_R) \sim R^{d-1}$;

2. Class II: $\sigma_N^2(\Omega_R) \sim R^{d-1} \log R$;

3. Class III: $\sigma_N^2(\Omega_R) \sim R^{d-\alpha}$, where $0 < \alpha < 1$.

In our analysis, we consider class-I hyperuniform point patterns that we generate using uniformly randomized lattices (URL) following the procedure in Ref. [30]:

1. Start with a perfect two-dimensional (2D) square lattice in a square simulation box with side length L and periodic boundary conditions. Such a lattice has strongly suppressed long-wavelength density fluctuations and thus is class-I hyperuniform. Crystals are ordered and hence are trivially class-I hyperuniform.

2. Shift each lattice point $\mathbf{r}_i = (x_i, y_i)$ by a vector $\boldsymbol{\delta}_i = (\delta_{i,x}, \delta_{i,y})$, where we draw each entry of a vector from a uniform distribution on $[-a/2, a/2]$. The perturbation strength a controls the maximum displacement and allows one to tune a system from near-lattice configurations to increasingly disordered configurations. The space between adjacent points of the lattice is 1, so a is a dimensionless parameter that encodes the disorder strength in units of the lattice spacing.

For perturbation strengths $a \approx 0$, we obtain a configuration that is almost a perfect lattice. These configurations have very little translational disorder. As we increase a, the local translational disorder grows, yet the point pattern remains hyperuniform [30]. Accordingly, we refer to the perturbation strength a as a "disorder strength".

III. METHODS

A. Point-pattern generation

We generate ensembles of class-I URL point patterns for 20 values of the disorder strength a inside a square periodic domain $[0, L] \times [0, L] \subset \mathbb{R}^2$. To have a nonhyperuniform baseline to use for comparisons, we also generate Poisson point patterns by uniform sampling in the same domain. We examine system sizes that range from configurations with 9 points (i.e., 3×3 lattices) to systems with 484 points (i.e., 22×22 lattices). We thereby cover a wide range of network sizes, and we are able to study finite-size effects and to ensure robust statistical sampling. For each system size, we generate Poisson point

patterns by uniformly random sampling in the same 2D periodic domain with the same number density as the corresponding URL patterns.

The Poisson patterns are nonhyperuniform, with number variances that scale linearly with the window volume (i.e., $\sigma_N^2(\Omega_R) \sim |\Omega_R|$ as $R \longrightarrow \infty$), in contrast to the suppressed fluctuations in hyperuniform systems. In the present paper, we systematically compare HuPPI and PoPPI networks for several network-generation methods (see Sec. III B). Throughout the present paper, we use the term "system size" to mean the number of points (N) in a point pattern, and we use the term "network size" to mean the number of nodes (n) in a network.

B. Network generation

There are numerous models of random tessellations [31]. In our study, we construct four types of planar networks (and associated tessellations) from the 2D point patterns that we described in Sec. III A. For each point pattern $P = \{\mathbf{p}_1, \mathbf{p}_2, \ldots, \mathbf{p}_N\} \subset \mathbb{R}^2$, we generate four families of networks.

1. **Delaunay tessellation [2]**: We consider each set $\{\mathbf{p}_i, \mathbf{p}_j, \mathbf{p}_k\} \subset P$ of three points, and we form edges between each pair of points in the set to form a triangle $[\mathbf{p}_i, \mathbf{p}_j, \mathbf{p}_k]$ if and only if the circumscribed circle of the set includes no other points from P in its interior.

2. **Gabriel graphs [2]**: We connect two points $\mathbf{p}_i$ and $\mathbf{p}_j$ if and only if the closed disk whose diameter is the line segment $\overline{\mathbf{p}_i \mathbf{p}_j}$ includes no other points from P. We refer to this disk as a *diametral disk* and to the requirement that there are no other points from P within it as an "empty-disk requirement". A Gabriel graph is a subgraph of a Delaunay tessellation.

3. **Voronoi tessellation [2]**: In a periodic square domain $[0, L] \times [0, L] \subset \mathbb{R}^2$, the Voronoi cell V_i of each point $\mathbf{p}_i \in P$ is the set of all points $\mathbf{x} \in [0, L] \times [0, L]$ that are closer to $\mathbf{p}_i$ than to any other point in P. That is, $V_i = \{\mathbf{x} \in [0, L] \times [0, L] \mid \|\mathbf{x} - \mathbf{p}_i\| \leq \|\mathbf{x} - \mathbf{p}_j\| \text{ for all } j \neq i\}$. Each node is attached (i.e., "incident") to exactly three edges, so the resulting graph is 3-regular. The three edges that meet at any node intersect only at that node, so incident edges never overlap along their interiors. We use the term "tree-like" to describe this degree-three local geometry, which is responsible for the predominantly negative ORCs that we observe in Voronoi networks.

4. **Delaunay-centroidal tessellation [18]**: We first compute the Delaunay tessellation of a point pattern. For each of its triangles $[\mathbf{p}_{i_1}, \mathbf{p}_{i_2}, \mathbf{p}_{i_3}]$, we then

compute the centroid $\mathbf{c}_{i_1,i_2,i_3} = \frac{1}{3}\sum_{m=1}^{3}\mathbf{p}_{i_m}$. We connect two such centroids if and only if their corresponding triangles share a common edge in the Delaunay tessellation. Because each triangle has exactly three edges, each centroid is adjacent to precisely three neighbors, yielding a 3-regular graph in which the edges that are incident to any node intersect only at that node. This tree-like structure also leads to most edges having negative ORCs.

These four generation methods yield networks with distinct connectivity patterns even when they have the same underlying point pattern. To compare their transport properties on equal footing, we will prescribe a common weighting scheme. We treat every network as undirected and assign edge conductances that depend solely on edge lengths.

For the Delaunay-centroidal and Voronoi constructions, it is crucial to distinguish the nodes of the final network from the points of the initial point pattern. In a Delaunay-centroidal network, the nodes are the centroids of the Delaunay triangles. In a Voronoi network, the nodes correspond to the circumcenters (i.e., the centers of the circumscribed circles) of the Delaunay triangles. For both Delaunay-centroidal networks and Voronoi networks, the number n of nodes is directly related to the number N of points of the point pattern by the Euler-characteristic formula for a torus [32]. For a generic configuration, this yields the expression $n = 2N$. The fact that these two network-generation methods generate networks with twice as many nodes as in the original point pattern is a key difference between them and the Delaunay and Gabriel constructions, for which $n = N$ because the points themselves become the nodes.

Given a graph $G = (V, E)$ that is embedded in a square domain with periodic boundaries, a "cell" is a connected open set $C \subset \mathbb{R}^2$ whose boundary ∂C is a simple closed polygon with edges from the set E. Distinct cells have disjoint interiors, and the union of their closures covers the domain, so the cells are precisely the 2D faces between the nodes and edges of G. In a Delaunay triangulation, each triangular face is a cell. In a Gabriel graph, the cells are the bounded faces (which need not be triangles) in its embedding. Each Voronoi region is a cell. The cells of a Delaunay-centroidal network are the bounded faces that one obtains by connecting the centroids of a Delaunay triangulation, with each cell of the Delaunay-centroidal network centered on a node in the Delaunay triangulation.

C. Network analysis

1. Edge weights and conductance

For each edge $(i,j) \in E$ of a network, we assign a conductance to give a weight $w_{ij} = 1/\ell_{ij}$, where ℓ_{ij} is the Euclidean length of the edge. With this weighting, shorter edges have larger conductances, which is physi-

cally sensible for transport processes. We use this choice of weighting throughout our analysis of network properties.

2. System size and dimensionality

All of our point patterns and networks live in a 2D space. The number of points (i.e., the system size N) in the original point pattern need not match the number of nodes (i.e., the network size n) in the resulting network, and such mismatches occur particularly for the Voronoi and Delaunay-centroidal networks. For instance, in a Delaunay-centroidal network, each triangle contributes one centroidal node, so the total node count can exceed the number of points in the original point pattern.

3. Periodic boundary conditions

Because we seek to study large-scale density fluctuations and avoid finite-size effects at the boundaries, we impose periodic boundary conditions for all point patterns prior to generating networks from them. Concretely, we identify (1) the left and right boundaries of the square domain and (2) the top and bottom boundaries of the square domain, effectively "wrapping" the system to form a torus. Consequently, the edges in the Gabriel, Delaunay, Delaunay-centroidal, and Voronoi networks can connect points that lie near opposite sides of our computational box.

4. Network ensembles and sampling

For each set of parameters (i.e., system size, disorder strength a, and point-pattern type), we generate an ensemble of point patterns and then construct the corresponding Delaunay, Gabriel, Voronoi, and Delaunay-centroidal networks. For each situation, we create 100 realizations so that we can compute reliable sample means and variances of our subsequent measurements. In the results that we report, each data point reflects statistics from many independent realizations of the same conditions, enabling us to probe how hyperuniform and nonhyperuniform point patterns affect network geometry and transport on average.

C. Network analysis

1. Ollivier–Ricci curvature (ORC)

ORC assigns each edge a measure of local network geometry by comparing the cost of transporting probability mass between the neighborhoods of the nodes that are attached to it [26, 27]. Let $d(i,j)$ denote the shortest-path

distance between nodes i and j. We equip each node i with the probability measure

$$m_i(z) = \begin{cases} \dfrac{w_{iz}}{\sum_{z' \in \mathcal{N}(i)} w_{iz'}}, & z \in \mathcal{N}(i) \\ 0, & \text{otherwise}, \end{cases} \quad (3)$$

where $\mathcal{N}(i)$ is the set of all nodes that are adjacent (i.e., connected directly) to node i (not including i itself) and w_{iz} is the weight of edge (i, z).

For nodes i and j, the 1-Wasserstein distance [33] between the probability measures m_i and m_j is

$$W_1(m_i, m_j) = \inf_{\Pi \in \Gamma(m_i, m_j)} \sum_{u,v} \Pi(u, v)\, \rho(u, v), \quad (4)$$

where $\Gamma(m_i, m_j)$ is the set of all admissible transport plans between probability measures m_i and m_j, the quantity $\Pi(u, v)$ is the amount of probability mass that is transported from point u to point v under a specific transport plan Π, and $\rho(u, v)$ is the length of a shortest path between u and v. A "transport plan" Π, which is a concept from the theory of optimal transport, is a joint probability measure over pairs of nodes that prescribes how much probability mass to move from each source u to each target v [33]. In the set $\Gamma(m_i, m_j)$ of admissible plans, the probability measures m_i and m_j are the marginals of Π. The ORC of the edge (i, j) is

$$\kappa(i, j) = 1 - \frac{W_1(m_i, m_j)}{d(i, j)}. \quad (5)$$

Edges with $\kappa \approx 1$ indicate redundancies in the network connectivity, whereas very negative values of κ indicate bottlenecks to transport. In Sec. V, we compute the ORC κ for the edges of our networks and analyze the resulting ORC distributions to compare our network-generation methods and the consequences of their underlying point patterns.

2. Total effective resistance (TER)

One can examine the transport efficiency in a network using the lens of electrical resistance [34], where one treats a network as an electrical circuit with its edges as resistors. In this analogy, the total effective resistance (TER) $\mathcal{R}_{\text{tot}}$ measures how easily current (or some other transported quantity) can flow through a network. A smaller TER indicates better overall connectivity and more efficient transport, as it implies that there are more redundant paths between nodes and fewer bottlenecks along those paths [24]. Therefore, computing TER is useful for comparing different network structures by providing a single value to quantify a graph's overall resistance [24]. One can compute TER to compare the robustness of networks by evaluating how their resistance changes in response to component failures [35]. In the context of

network design, one can treat TER as an objective function to minimize to obtain an efficient graph structure for transport [36].

We determine TER from the combinatorial graph Laplacian matrix $\mathbf{L}$ [37], which encodes a network's connectivity structure. The entries of $\mathbf{L}$ are

$$L_{ij} = \begin{cases} \sum_k w_{ik}, & i = j \\ -w_{ij}, & i \neq j \text{ and } (i, j) \in E \\ 0, & \text{otherwise}. \end{cases} \quad (6)$$

Let $\mathbf{L}^+$ denote the Moore–Penrose pseudoinverse of $\mathbf{L}$ [38], and let $\mathbf{e}_i$ and $\mathbf{e}_j$ denote unit vectors (with 1 in the ith and jth entries, respectively, and 0 in all other entries) that select the corresponding nodes. The resistance between nodes i and j is

$$R_{ij} = (\mathbf{e}_i - \mathbf{e}_j)^{\mathsf{T}} \mathbf{L}^+ (\mathbf{e}_i - \mathbf{e}_j), \quad (7)$$

and the TER is

$$\mathcal{R}_{\text{tot}} = \frac{1}{2} \sum_{i,j} R_{ij} = n \operatorname{Tr}(\mathbf{L}^+), \quad (8)$$

where n is the number of nodes and Tr denotes the trace of a matrix.

3. Random-walk mixing time

For a standard random walk on a weighted, undirected graph with node set $\{1, \ldots, n\}$, let $w_{ij} = w_{ji} \geq 0$ be the weight of edge (i, j) and define the strength (i.e., weighted degree) of node i by $d_i = \sum_{j=1}^{n} w_{ij}$. The transition matrix of a standard random walk is $\mathbf{P} = \mathbf{D}^{-1}\mathbf{A} = \mathbf{I} - \mathbf{D}^{-1}\mathbf{L}$, where $\mathbf{A} = (w_{ij})$ is the weighted adjacency matrix, $\mathbf{D} = \operatorname{diag}(d_1, \ldots, d_n)$ is the diagonal matrix of strengths, and $\mathbf{L} = \mathbf{D} - \mathbf{A}$ is the combinatorial graph Laplacian [37, 39]. [See Eq. (6) for the entries of $\mathbf{L}$.] The stationary distribution of $\mathbf{P}$ has entries

$$\pi_i = \frac{d_i}{\sum_{k=1}^{n} d_k}. \quad (9)$$

The total-variation (TV) distance after t steps from a starting node i is

$$\left\| \mathbf{P}^t(i, \cdot) - \boldsymbol{\pi} \right\|_{\text{TV}} = \frac{1}{2} \sum_j \left| \mathbf{P}^t(i, j) - \pi_j \right|, \quad (10)$$

and the ϵ-mixing time [25, 39] is

$$\tau_{\text{mix}}(\epsilon) = \min \left\{ t : \max_i \left\| \mathbf{P}^t(i, \cdot) - \boldsymbol{\pi} \right\|_{\text{TV}} \leq \epsilon \right\}. \quad (11)$$

The ϵ-mixing time is the minimum number of steps that it takes for a random walk on a network to get sufficiently "close" to its stationary distribution when it starts from

the worst possible initial node. More precisely, the ϵ-mixing time is the smallest time t such that the probability distribution of a walk after t steps is within TV-distance ϵ of the stationary distribution regardless of where the walk started.

A common convention is to use $\epsilon = 1/4$ [39], but we adopt a stricter convergence criterion to reduce the variance in our numerical computations. In Sec. VI, we calculate $\tau_{\mathrm{mix}}(\epsilon)$ for $\epsilon = 10^{-3}$ for our networks and thereby corroborate the transport picture that we infer by calculating ORCs and TERs.

4. Robustness

We track the evolution of the size of the largest connected component (LCC) of a network relative to its total number of nodes as we progressively remove edges from it. We consider a network to be more robust than another network if its LCC retains a larger fraction of its nodes for the same fraction of removed edges [40, 41].

We assess network robustness by examining the change in the size (i.e., number of nodes) of its LCC as we sequentially remove edges using different strategies. We consider two edge-removal strategies: (1) random removal, in which we remove edges uniformly at random; and (2) targeted removal, in which we remove edges in the order of their ORC values, starting with the most negative (i.e., most bottleneck-like) edges. After each edge removal, we recompute the size of the LCC and track its size (relative to the overall network size) as a function of the fraction of edges that we have removed. All of our statistics are means of 20 independent realizations of the original networks.

IV. CALCULATIONS OF GLOBAL MEASURES

We now examine TER and random-walk mixing time as a function of the disorder strength a of the HuPPI networks.

A. Total effective resistance (TER) $\mathcal{R}_{\mathrm{tot}}$

When plotting results for TER, it is convenient to normalize the TER $\mathcal{R}_{\mathrm{tot}}$ by defining

$$\mathcal{R}_{\mathrm{norm}} = \frac{\mathcal{R}_{\mathrm{tot}}}{n^2 \ln n} \tag{12}$$

because the factor $n^2 \ln n$ is the leading-order growth of the TER for a square-lattice network with periodic boundary conditions [42, 43]. Although our HuPPI and PoPPI graphs are not square lattices, they are embedded in a 2D space with periodic boundary conditions. In our empirical calculations, we observe that scaling $\mathcal{R}_{\mathrm{tot}}$ by $n^2 \ln n$ results in a value that is approximately constant
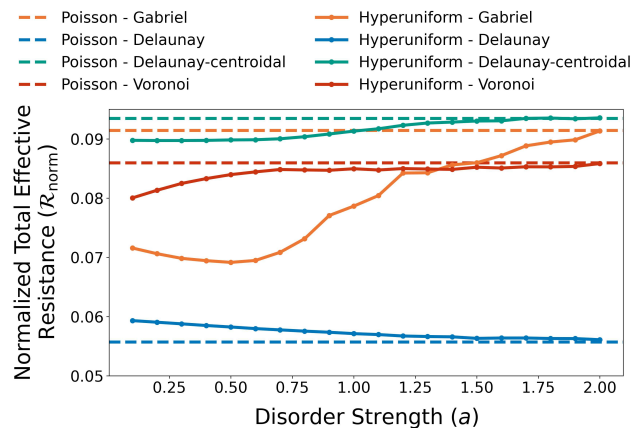

FIG. 1. Normalized total effective resistance (TER) $\mathcal{R}_{\mathrm{norm}}$ as a function of disorder strength a for HuPPI networks (solid curves) and PoPPI networks (dashed curves) for Gabriel, Delaunay, Delaunay-centroidal, and Voronoi networks. We generate these networks from 15×15 lattices (which have 225 points). Smaller normalized TERs indicate the presence of more redundant paths and hence better connectivity.
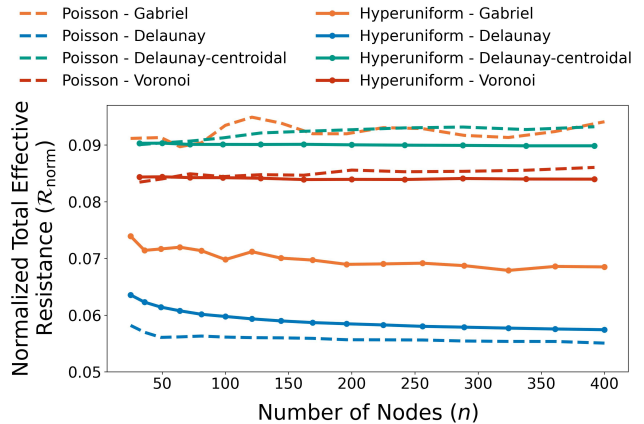

FIG. 2. Normalized TER $\mathcal{R}_{\mathrm{norm}}$ versus the network size (i.e., number of nodes) n for HuPPI networks (solid curves) and PoPPI networks (dashed curves) for Gabriel, Delaunay, Delaunay-centroidal, and Voronoi networks. The HuPPI networks, which we generate from hyperuniform point patterns, have a disorder strength of $a = 1$. As we increase n, it becomes easier to distinguish between the curves for the hyperuniform and random point patterns.

across system sizes and network types. (Simpler scaling choices do not gives us a value that is approximately independent of system size.) In particular, we observe that $\mathcal{R}_{\mathrm{norm}}$ behaves as an intensive transport measure of transport for the examined networks.

In Figs. 1 and 2, we illustrate how normalized TER $\mathcal{R}_{\mathrm{norm}}$ varies with the disorder strength a and the network size n. Except for the Delaunay networks, we observe that the HuPPI networks have smaller TERs than PoPPI networks, reflecting the former's more uniform coverage in space that suppresses large voids between
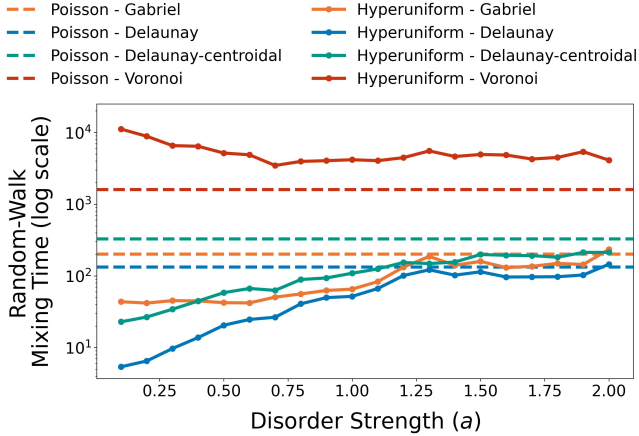
FIG. 3. Random-walk mixing time as a function of the disorder strength a for HuPPI networks (solid curves) and PoPPI networks (dashed curves) for Gabriel, Delaunay, Delaunay-centroidal, and Voronoi networks. We generate networks from 15×15 lattices (which have 225 points). By definition, the PoPPI networks do not depend on a.

points. By contrast, Poisson point patterns can generate extended spatial regions with no nodes or edges. In an undirected network, when there are such regions, current (or some other quantity) that flows between many origin–destination node pairs has to detour along longer paths, and the resulting larger pairwise effective resistances accumulate to inflate the TER $\mathcal{R}_{\text{tot}}$.

The Voronoi and Delaunay-centroidal networks tend to have larger $\mathcal{R}_{\text{norm}}$ values than the Gabriel and Delaunay networks because the tree-like connections in the former two types of networks limit their numbers of redundant paths. In Delaunay, Delaunay-centroidal, and Voronoi networks, the total number of edges is determined solely by the system size, so the edge count is the same for all network realizations. By contrast, different Gabriel graphs with the same system size have different numbers of edges. Consequently, Gabriel graphs have noticeably higher variabilities in $\mathcal{R}_{\text{norm}}$ (see Figs. 1 and 2) than the other three types of networks.

B. Random-walk mixing time

We also measure how fast a standard random walk on a network approaches its stationary distribution. We quantify this convergence speed by calculating the ϵ-mixing time $\tau_{\text{mix}}(\epsilon)$, which we recall (see Sec. III C 3) is the minimum number of steps t such that the TV distance between the walk's distribution after t steps and the stationary distribution is at most ϵ. Smaller random-walk mixing times indicate more efficient linear diffusion in a network. In Fig. 3, we show the random-walk mixing times for each network-generation method for both HuPPI and PoPPI networks.

For Gabriel, Delaunay, and Delaunay-centridal graphs,

the HuPPI networks require fewer steps to reach stationarity than their PoPPI counterparts. This improvement arises because HuPPI networks have fewer sparsely connected regions and a more even spatial distribution of edges, which together shorten the "hitting time" (i.e., the expected number of steps that it takes for a random walk starting from the worst initial node to reach an arbitrary target node) [39]. A smaller maximum hitting time directly translates into a smaller mixing time, so the enhanced local connectivity of HuPPI networks accelerates global convergence. Moreover, the choice of network-generation method can overshadow differences between HuPPI and PoPPI networks. For instance, a dense Delaunay network can have faster random-walk mixing than a sparse Gabriel graph for both types of point patterns.

For the Voronoi networks, the HuPPI and PoPPI networks have different random-walk mixing times. In particular, the HuPPI networks have larger random-walk mixing times than PoPPI networks for all perturbation strengths a. This may be due to the abundance of very short edges in the HuPPI Voronoi networks. These edges have large weights, so intuitively they dominate random-walk transitions. Consider the transition probability P_{ij} from node i to node j. If nodes i and j are adjacent, the transition probability is

$$P_{ij} = \frac{w_{ij}}{\sum_k w_{ik}} = \frac{\frac{1}{\ell_{ij}}}{\sum_k \frac{1}{\ell_{ik}}} . \qquad (13)$$

When few edges are very short, their associated weights are very large, so such edges attract much of the probability flow. Consequently, the HuPPI Voronoi networks take longer to converge to the stationarity distribution than PoPPI Voronoi networks.

V. OLLIVIER–RICCI CURVATURE (ORC): A LOCAL MEASURE

A. ORC distributions

In Fig. 4, we show the ORC distributions for both HuPPI and PoPPI networks. Our observations underscore the fact that both the underlying point-pattern type (hyperuniform versus Poisson point patterns) and the specific type of network (Gabriel and Delaunay networks versus Delaunay-centroidal and Voronoi networks) jointly influence the shape of the ORC distribution. The PoPPI networks have a slightly wider spread of curvatures than the HuPPI networks. The choice of network-generation method further influences this general distinction. For instance, the Delaunay networks have larger ORCs than the other types of networks because they are denser than the other types of networks. By contrast, many edges in Voronoi and Delaunay-centroidal networks link two nodes whose neighbor sets have few or no common members (other than those nodes themselves). This weak overlap in neighborhoods yields more

negative ORCs than in Delaunay or Gabriel networks.

We also observe that the Delaunay and Gabriel networks have similar ORC distributions. Recall that a Gabriel graph is a subgraph of a Delaunay graph, so every Gabriel edge is also a Delaunay edge, whereas any Delaunay edge whose diametral disk has additional points is not in its associated Gabriel subgraph. The Delaunay and Gabriel constructions both connect points based on an empty-disk requirement (via circumscribed circles for Delaunay networks and diametral disks for Gabriel networks), so they have similar local connectivity patterns. Therefore, the edges throughout these networks have neighborhoods with similar local geometries. Consequently, for both Delaunay and Gabriel constructions, the HuPPI networks have narrower ORC distributions than the corresponding PoPPI networks, which have more variable edge densities due to the density fluctuations in Poisson point patterns.

The Voronoi and Delaunay-centroidal networks appear to have bimodal ORC distributions. Voronoi networks have cell boundaries without a dense triangle structure that is typical of Delaunay networks (and partially inherited by Gabriel networks). Therefore, some edges can link triangles that share elongated boundaries (potentially driving ORCs towards more negative values), while other edges remain short and highly clustered (pushing ORCs towards 0 or even positive values). Similarly, a Delaunay-centroidal network, which connects the centroids of Delaunay cells, also possesses edges that are significantly longer than Delaunay edges that one obtains from the the same point pattern, as edges sometimes skip nearest neighbors and instead link more distant nodes. We believe that this edge heterogeneity is what yields the bimodality in the ORC distributions.

B. Mean ORC versus disorder strength a

We now examine how the disorder strength a affects the mean ORC. We show our results in Fig. 5. As we increase a from nearly lattice-like configurations (i.e., very small a) to more perturbed configurations, the mean ORCs in the HuPPI networks progressively approach the mean ORCs in the corresponding PoPPI networks. For disorder strengths near $a \approx 0.75$, the mean ORCs in the HuPPI networks are smaller than the mean ORCs in the corresponding PoPPI networks for all four network types. For some network types, this disparity is prominent for a wide range of disorder strengths. As we increase a beyond $a \approx 1.5$, the network properties (including the mean ORCs) of the HuPPI networks converge to values that are indistinguishable from those in PoPPI networks, even though the underlying point patterns remain hyperuniform (as one can verify by measuring their density fluctuations). In other words, the network-generation process becomes less sensitive to the underlying hyperuniformity as we increase the disorder strength a.

We also see in Fig. 5 that the network-generation method has a large effect on the mean ORC. For instance, the Delaunay networks tend to have edges with larger ORCs than the Gabriel and Delaunay-centroidal networks, so the Delaunay networks' curve of mean ORC versus disorder strength a lies above the curves for the other networks. We also observe that the Voronoi and Delaunay-centroidal networks have a prominent nonmonotonic dependence on the disorder strength a that does not occur in the other types of networks. (The Gabriel graphs do have a slight nonmonotonic dependence.) For small a, the mean ORCs of the HuPPI Voronoi networks is positive (it is roughly +0.1) and it is larger than that for the corresponding PoPPI Voronoi networks. As we increase a, the mean ORCs of the HuPPI Voronoi networks drops below the mean ORCs in the PoPPI Voronoi networks, and it eventually converges from below to the same limiting value for sufficiently large a. For very small a (i.e., in the near-lattice regime), there are extremely short edges along the boundaries of the Voronoi cells. These short edges yield local connectivity patterns with positive-ORC edges. As we increase a (i.e., as the lattice structure becomes more perturbed), such very short edges typically disappear and there instead are longer edges, which have smaller ORCs than the very short edges. Therefore, as we increase the disorder strength a, the mean ORC in HuPPI networks crosses below the PoPPI mean ORC and later rises to asymptotically approach it again for large a.

C. Convergence of Mean ORC with increasing network size

We also examine how ORC changes with network size (i.e., number of nodes) n. In Fig. 6, we plot the mean ORC versus n. For networks with roughly 100 or more nodes, the mean ORCs stabilize, and we no longer need to worry about finite-size fluctuations. This is a promising observation for analyzing ORCs in physical networks that one constructs experimentally in laboraties (e.g., via additive manufacturing [44]), as it suggests that even modest network sizes are sufficient for stable ORC estimates [3]. Additionally, we observe for all network sizes that HuPPI networks consistently have smaller mean ORCs than PoPPI networks, although the difference is sometimes small. Furthermore, we observe that the network-generation method can shift ORCs up or down more strongly than any differences that arise due to differences between hyperuniform and Poisson point patterns.

D. Edge-level correlations between ORC and TER

Comparing our global-transport results (see Sec. IV) with the local-curvature statistics reveals a counterintuitive situation. Negative ORC typically indicates the presence of bottlenecks [26, 45–47], so one may expect
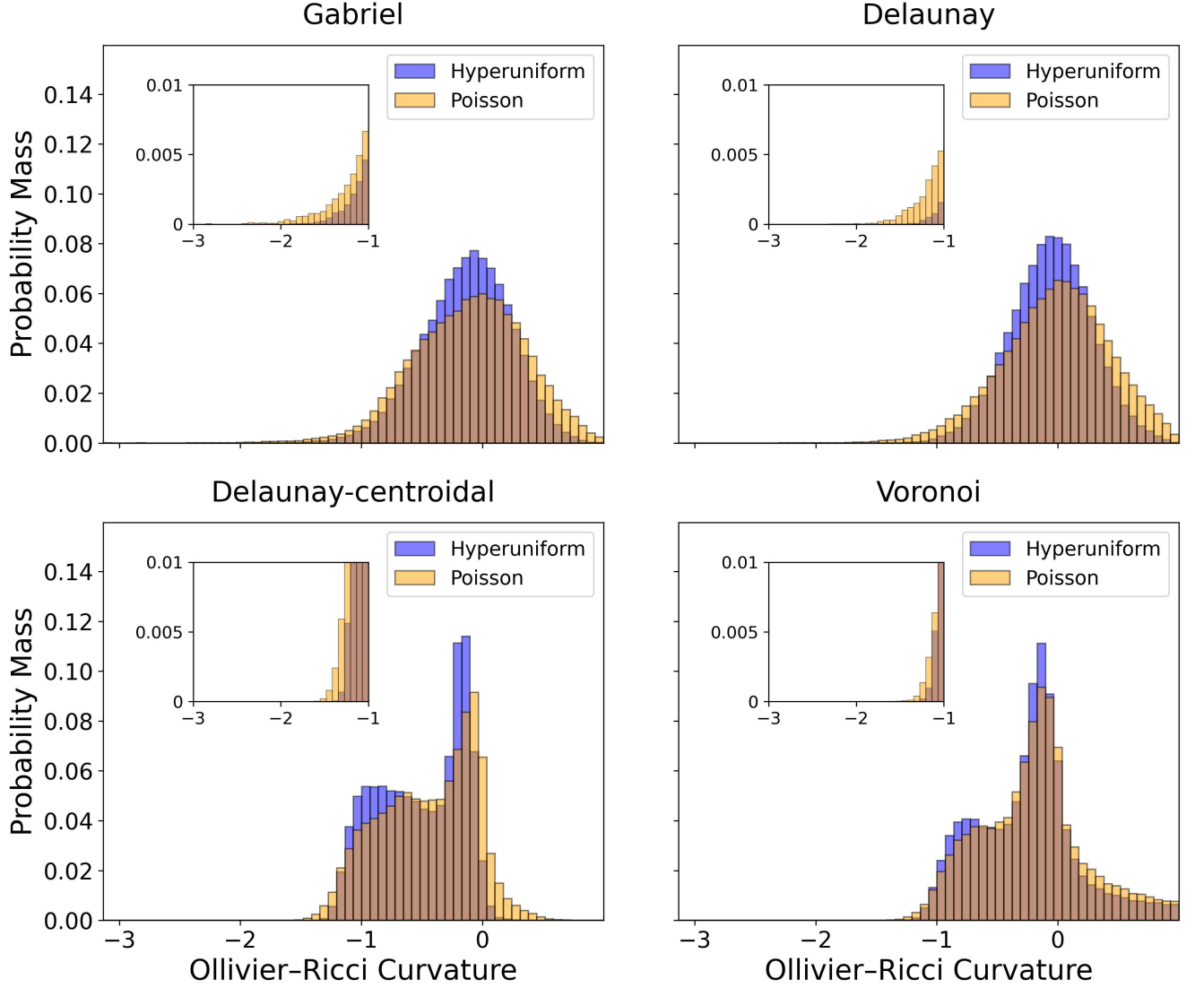
FIG. 4. Histograms of ORCs for HuPPI networks (blue) with disorder strength $a = 1$ and PoPPI networks (orange) for Gabriel, Delaunay, Delaunay-centroidal, and Voronoi networks. We generate these networks from 15×15 square lattices (which have 225 points). The histograms aggregate data from five independent realizations of each type of point pattern.

that networks with more negative mean curvatures have larger TERs. However, we instead observe the opposite scenario: HuPPI networks simultaneously have more negative mean ORCs (see Fig. 5) and smaller TERs (see Fig. 1) than PoPPI networks. To resolve this counterintuitive situation and gain insights into how local geometry impacts TER, we analyze the relationship between the ORC $\kappa(e)$ of an individual edge e and its specific contribution to TER. We calculate the *TER edge contribution*

$$\Delta\mathcal{R}_{\text{tot}}(e) = \mathcal{R}_{\text{tot}}(G \setminus \{e\}) - \mathcal{R}_{\text{tot}}(G), \qquad (14)$$

where $\mathcal{R}_{\text{tot}}(G \setminus \{e\})$ is the TER of a network after removing edge e and $\mathcal{R}_{\text{tot}}(G)$ is the TER of the original network. In Fig. 7, we show scatter plots for point patterns with $N = 1089$ points.

The relationship between the edge-level ORC $\kappa(e)$ and the TER edge contribution $\Delta\mathcal{R}_{\text{tot}}(e)$ is complex and depends on the method of network generation. For each network type, we compute the Pearson correlation coefficient r between $\kappa(e)$ and $\Delta\mathcal{R}_{\text{tot}}(e)$ across 10 independent realizations and report the mean value. For HuPPI networks, we find $r \approx 0.0857$ for Gabriel networks, $r \approx 0.6177$ for Delaunay networks, $r \approx -0.4853$ for Delaunay-centroidal networks, and $r \approx 0.0682$ for Voronoi networks. For PoPPI networks, the mean correlations are $r \approx 0.0222$ for Gabriel networks, $r \approx 0.3441$ for Delaunay networks, $r \approx -0.2153$ for Delaunay-centroidal networks, and $r \approx 0.0904$ for Voronoi networks. Notably, the strong positive correlation in Delaunay networks seems counterintuitive, as one may expect a negative edge-level ORC
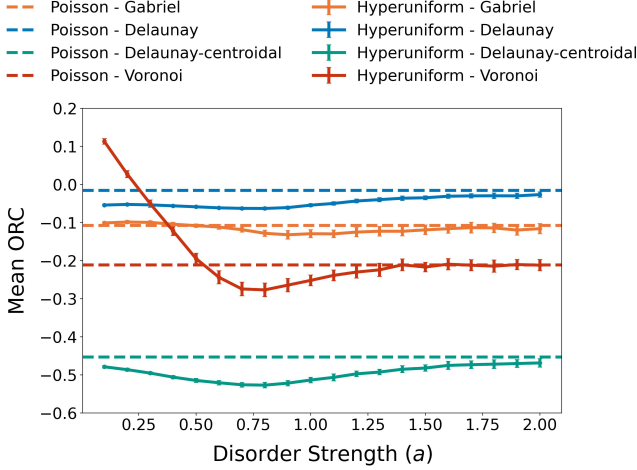
FIG. 5. Mean ORC as a function of disorder strength a for HuPPI networks (solid curves) and PoPPI networks (dashed curves) for Gabriel, Delaunay, Delaunay-centroidal, and Voronoi networks. We generate these networks from 15×15 square lattices (which have 225 points). For each type of HuPPI network, the curves give mean ORCs for 50 independent realizations, with error bars indicating one standard deviation from the mean.
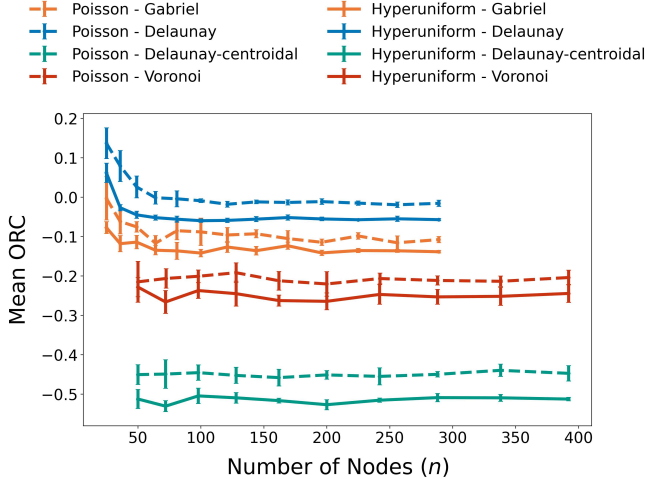

FIG. 6. Mean ORC versus network size (i.e., number of nodes) for HuPPI networks (solid curves) with disorder strength $a = 1$ and PoPPI networks (dashed curves) for Gabriel, Delaunay, Delaunay-Centroidal, and Voronoi networks. The curves give mean ORCs for 50 independent realizations, with error bars indicating one standard deviation from the mean.

$\kappa(e)$ to entail a large TER edge contribution $\Delta\mathcal{R}_{\text{tot}}(e)$. We believe that this counterintuitive situation arises because both $\Delta\mathcal{R}_{\text{tot}}(e)$ and $\kappa(e)$ depend strongly on the edge length ℓ_{ij}. In a Delaunay network, longer edges tend to have both a smaller $\Delta\mathcal{R}_{\text{tot}}(e)$ and more negative curvature (as they often bridge clusters and share fewer neighbors than shorter edges). The counterintuitive correlation in Delaunay networks illustrates that the contri-

bution of a single edge to TER is not a straightforward proxy for an edge's role as a structural bottleneck for all network types. Despite the inconsistent correlations, Fig. 7 gives visual confirmation of the above conceptual explanation. The PoPPI scatter plots are significantly more dispersed than the HuPPI plots. This visualizes the large spread of curvatures in PoPPI networks. Crucially, the dispersion in PoPPI networks leads to outlier edges with very large $\Delta\mathcal{R}_{\text{tot}}(e)$ (as one can see in the large vertical dispersions in Fig. 7). These outliers correspond to critical bridges, as removing them from a network severely disrupts global transport. The disorder strength in Fig. 7 is $a = 1$, so we do not observe outliers in the HuPPI networks. This small set of bridging edges elevates the TER $\mathcal{R}_{\text{tot}}$ of PoPPI networks. This absence of bridging edges in HuPPI networks resolves the counterintuitive situation that we described at the beginning of the present subsection. Although the mean ORCs in the HuPPI networks are more negative than the mean ORCs in the PoPPI networks, we now see that HuPPI networks lack the extreme bottleneck outliers that dominate TER in PoPPI networks. Consequently, we conclude that the smaller TERs in HuPPI networks than in PoPPI networks arise from the absence of edges with large $\Delta\mathcal{R}_{\text{tot}}(e)$ values rather than because HuPPI networks have more negative mean ORCs than PoPPI networks.

VI. ROBUSTNESS OF NETWORKS TO EDGE REMOVALS

We examine network robustness by progressively removing edges from our networks [40]. Our results are means of 20 independent realizations of each network type. We generate 20 independent realizations of each point pattern and then construct the four types of networks from each of these realizations. Cetinay et al. [48] demonstrated that targeting edges (or nodes) based on their curvatures or resistance-based centralities is able to identify structural bottlenecks in power-transmission networks, and they illustrated that removing such edges significantly disrupts network connectivity. Taking inspiration from their results, we consider two edge-removal strategies: (1) random removal, in which we remove edges uniformly at random; and (2) targeted removal, in which we remove edges in the order of their ORC values, starting with the edges with the most negative values (i.e., the most bottleneck-like). In our targeted-removal strategy, progressively removing the most bottleneck-like edges allows us to assess how quickly a network's connectivity degrades as one compromises the most important pathways through it.

For random edge removal [see Fig. 8(a)], the HuPPI Gabriel networks are consistently more robust than their PoPPI counterparts, with the HuPPI networks fragmenting significantly later than their PoPPI counterparts. For Delaunay networks, the advantage of hyperuniformity is more pronounced for targeted removal than for random
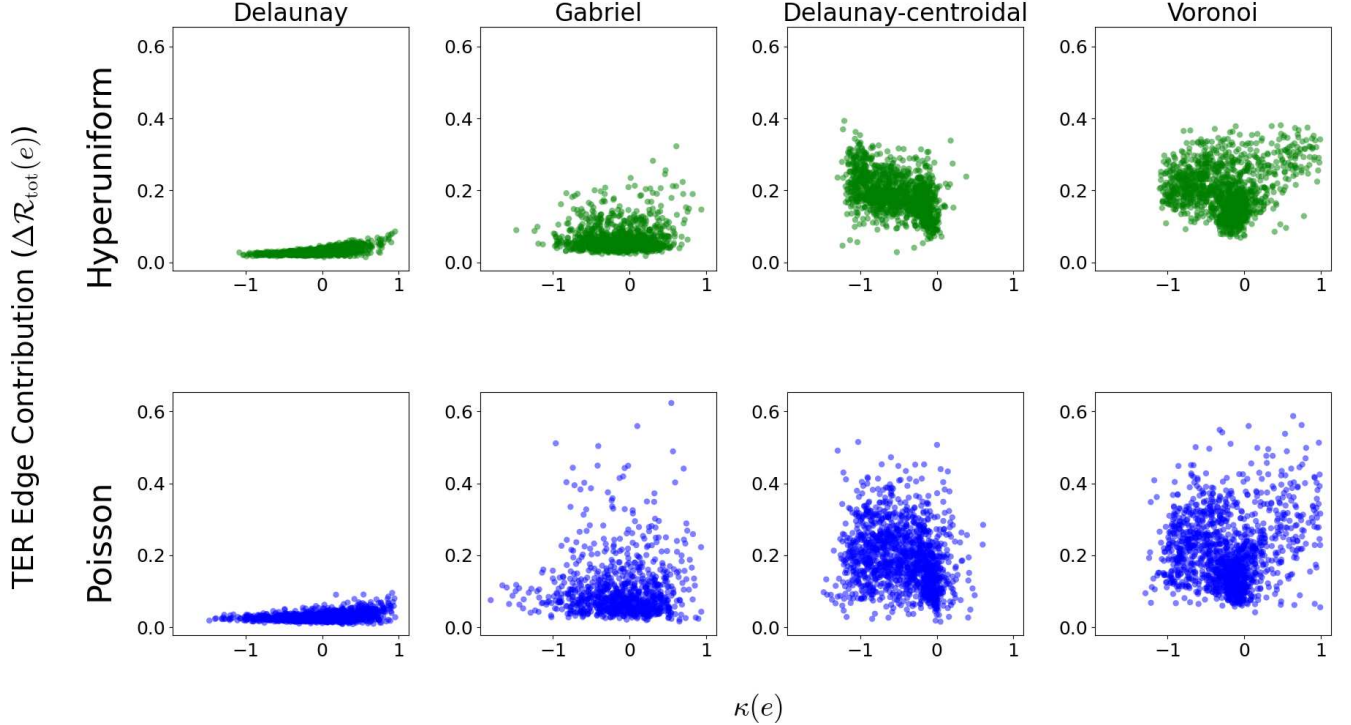
FIG. 7. Scatter plots of the edge-level ORC $\kappa(e)$ versus the TER edge contribution $\Delta\mathcal{R}_{\text{tot}}(e)$ of edges $e = (i, j)$ in (top) HuPPI networks with disorder strength $a = 1$ and (bottom) PoPPI networks for Delaunay, Gabriel, Delaunay-centroidal, and Voronoi networks (which we show from left to right). In each column, we show data from a single realization of both a HuPPI network and a PoPPI network. We generate each network from an initial point pattern with $33 \times 33 = 1089$ points.

edge removal. [see Fig. 8(b)]. PoPPI networks fragment much more rapidly than HuPPI in the Gabriel and Delaunay networks. However, HuPPI and PoPPI networks fragment similarly to each other for the Voronoi networks. Additionally, HuPPI networks fragment more rapidly than PoPPI networks for the Delaunay-centroidal networks.

VII. CONCLUSIONS AND DISCUSSION

We studied the influence of point-pattern hyperuniformity, which is characterized by the suppression of long-range density fluctuations in comparison to the fluctuations in standard disordered systems, on the structure of spatial networks. We calculated several global and local network measures — Ollivier–Ricci curvature (ORC) distributions, total effective resistance (TER), random-walk mixing times, and robustness to edge removal — in spatially embedded networks that we generated from both hyperuniform and Poisson point patterns.

Two key observations emerge from our numerical computations. First, although hyperuniform-point-pattern-induced (HuPPI) networks usually have smaller total effective resistances (TERs), slightly faster random-walk mixing times, and fewer extreme-curvature edges than Poisson-point-pattern-induced (PoPPI) networks, we observed that these differences do not arise from

the suppressed long-range density fluctuations in hyperuniform point patterns. Instead, they stem from subtle biases in local edge geometry that arise from the spatial correlations of the underlying point patterns. In particular, HuPPI networks have fewer extreme negative-curvature edges, which act as transport bottlenecks, than PoPPI networks. Second, the choice of network-generation method (Delaunay, Gabriel, Voronoi, or Delaunay-centroidal) is a key factor in the properties of the resulting networks.

The way that one determines the edges of a network can either amplify or mask the effects of local geometric biases. In our computations, we observed that a Delaunay triangulation and its Gabriel subgraph form a triangle-rich network family with high edge density and abundance short cycles that overlap between the neighborhoods of adjacent nodes. The high edge density and presence of short cycles suppresses extremely negative ORCs in the edges and yields smaller TERs (and hence high transport efficiencies) by providing many redundant short paths. Although the Gabriel network is not a pure triangulation, it inherits a high triangle density from the Delaunay triangulation, leading to similarly large ORCs and high transport efficiencies. By contrast, the Voronoi and Delaunay-centroidal networks are 3-regular graphs and have tree-like local structure, with few short cycles. Their structures accentuate extreme negative ORCs and increases the TER. These structural differences split our
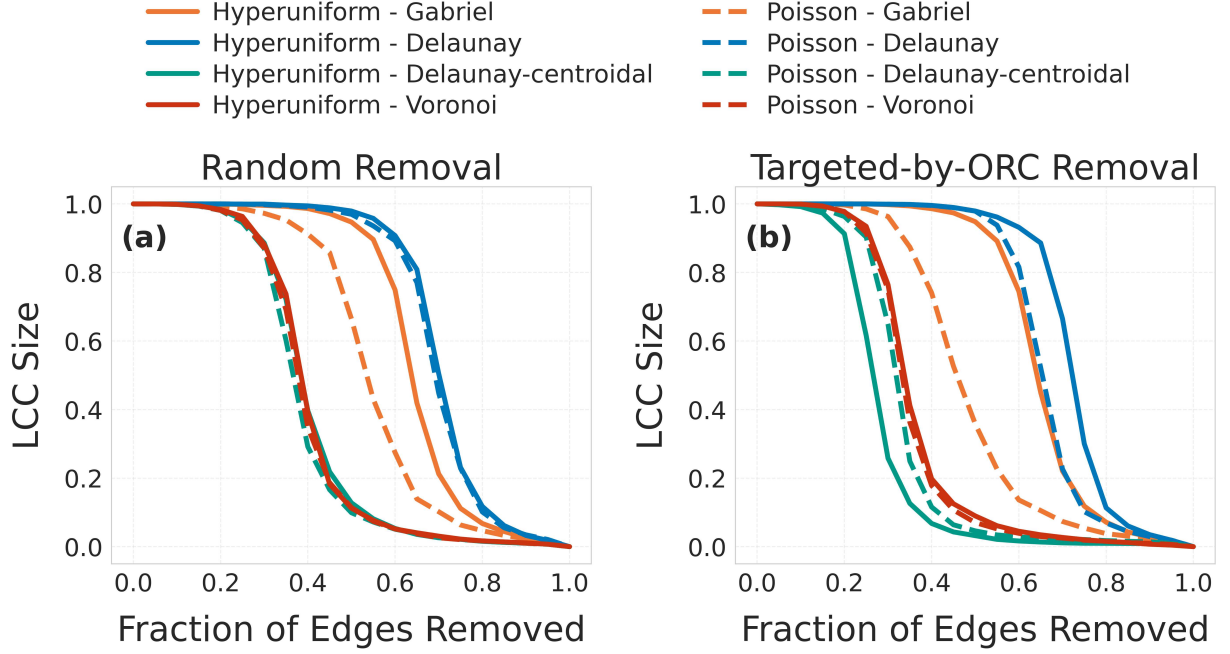
FIG. 8. Relative sizes of largest connected components (LCCs) of the networks versus the fraction of removed edges for two different removal strategies for HuPPI networks (solid curves) with disorder strength $a = 1$ and PoPPI networks (dashed curves) for Gabriel, Delaunay, Delaunay-centroidal, and Voronoi networks. We show results for (a) uniformly random removal of edges and (b) removal of edges in the order of their ORC values starting with the most negative value.

networks into two families: (1) Delaunay and Gabriel networks, which have triangle-rich connectivity and high local redundancy; and (2) Voronoi and Delaunay-centroidal networks, with sparse, tree-like local structure. As this classification underscores, the key differences that we observe in curvature and transport properties arise from the network-generation method rather than from whether the underlying point pattern is hyperuniform or Poisson. We also obtained the counterintuitive result that HuPPI networks simutaneously have smaller TERs $\mathcal{R}_{\mathrm{tot}}$ and more negative mean ORCs than their PoPPI counterparts In principle, edges with very negative ORCs act as bridge-like bottlenecks whose adjacent neighborhoods rarely overlap. Flows need to squeeze through these bridge-like edges, so one may expect a network with many such edges to have large pairwise effective resistances and hence a large TER. However, HuPPI networks have much narrower ORC distributions than PoPPI networks. In HuPPI networks, the edge-level ORCs are moderately negative on average and there are no outlier edges with very negative ORCs, so there are multiple pathways for efficient transport. Hyperuniformity thus reduces TER not by making edges have positive curvatures, but instead by reducing the presence of outlier edges with very negative ORCs that otherwise would dominate a network's TER. This counterintuitive outcome reflects the fact that PoPPI networks possess a small number of edges with very negative or very positive ORCs that dominate TER.

Overall, our computations indicate that hyperuniform point patterns can confer transport and robustness advantages over their Poisson counterparts in spatial networks that one generates from them. Importantly, however, we also observed that these advantages are not direct consequences of large-scale hyperuniformity but rather of their induced local geometric biases. The structure of HuPPI and PoPPI networks depends both on the correlations in their underlying point patterns and on the subsequent network-generation rules. These insights motivate (1) further theoretical efforts to relate curvature variance to transport measurements and (2) experimental studies that quantify how specific spatial point-pattern designs combine with particular network-generation rules to influence real-world performance.

Disordered systems offer a much larger design space than ordered systems, so it is important to examine how tuning the disorder strength in hyperuniform point patterns impacts the properties of the resulting HuPPI networks and other disordered metamaterials. Recent laboratory investigations of tunably disordered conductive and mechanical networks [3, 44], together with numerical investigations of network hyperuniformity [19], provide promising foundations for such work.

[1] M. Newman, *Networks*, 2nd ed. (Oxford University Press, Oxford, UK, 2018).

[2] M. Barthelemy, *Spatial Networks: A Complete Introduction: From Graph Theory and Statistical Physics to Real-World Applications* (Springer, Cham, Switzerland, 2022).

[3] C. Obrero, M. Tirfe, C. Lee, S. Saptarshi, C. Rock, K. E. Daniels, and K. A. Newhall, Phys. Rev. E **112**, 035505 (2025).

[4] M. Barthelemy and G. Boeing, Findings 10.32866/001c.122117 (2024).

[5] L. Cuadra, S. Salcedo-Sanz, J. Del Ser, S. Jiménez-Fernández, and Z. W. Geem, Energies **8**, 9211 (2015).

[6] J. Stiso and D. S. Bassett, Trends Cogn. Sci. **22**, 1127 (2018).

[7] J. Yang, S. A. Wagner, and P. Beli, Front. Genet. **6**, 344 (2015).

[8] R. Albert, B. DasGupta, and N. Mobasheri, Phys. Rev. E **89**, 032811 (2014).

[9] A. Liu and M. A. Porter, Phys. Rev. E **101**, 062305 (2020).

[10] M. Boguñá, I. Bonamassa, M. De Domenico, S. Havlin, D. Krioukov, and M. A. Serrano, Nat. Rev. Phys. **3**, 114 (2021).

[11] P. Calka, in *New Perspectives in Stochastic Geometry*, edited by W. S. Kendall and I. Molchanov (2009) pp. 145–170.

[12] Y. Yadav and K. Xia, arXiv preprint (2025), arXiv:2510.22599.

[13] K. Devriendt and R. Lambiotte, J. Phys. Complex. **3**, 025008 (2022).

[14] K. Devriendt, A. Ottolini, and S. Steinerberger, Disc. App. Math. **348**, 68 (2024).

[15] R. P. Sreejith, K. Mohanraj, J. Jost, E. Saucan, and A. Samal, Journal of Statistical Mechanics: Theory and Experiment **2016**, 063206 (2016).

[16] R. Lachièze-Rey, arXiv preprint (2025), arXiv:2510.18392.

[17] S. Torquato, Phys. Rep. **745**, 1 (2018).

[18] S. Torquato and D. Chen, Multifunct. Mater. **1**, 015001 (2018).

[19] C. E. Maher and K. A. Newhall, Phys. Rev. E **111**, 065420 (2025).

[20] E. Newby, W. Shi, Y. Jiao, R. Albert, and S. Torquato, Phys. Rev. E **111**, 034123 (2025).

[21] E. Newby, W. Shi, Y. Jiao, S. Torquato, and R. Albert, arXiv preprint (2025), arXiv:2504.01015.

[22] S. Torquato, J. Phys. Cond. Mat. **28**, 414012 (2016).

[23] J. Kim and S. Torquato, Phys. Rev. E **103**, 012123 (2021).

[24] W. Ellens, F. M. Spieksma, P. Van Mieghem, A. Jamakovic, and R. E. Kooij, Lin. Alg. Appl. **435**, 2491 (2011).

[25] R. Montenegro and P. Tetali, Found. Trend. Theor. Comp. Sci. **1**, 237 (2006).

[26] N. Azarhooshang, P. Sengupta, and B. DasGupta, Mathematics **8**, 1416 (2020).

[27] Y. Ollivier, in *Probabilistic Approach to Geometry*, Advanced Studies in Pure Mathematics, Vol. 57, edited by M. Kotani, M. Hino, and T. Kumagai (Mathematical Society of Japan, Tokyo, Japan, 2010) pp. 343–381.

[28] M. P. do Carmo, *Riemannian Geometry* (Birkhäuser, Basel, Switzerland, 1992).

[29] S. Torquato and F. H. Stillinger, Phys. Rev. E **68**, 041113 (2003).

[30] M. A. Klatt, J. Kim, and S. Torquato, Phys. Rev. E **101**, 032118 (2020).

[31] C. Redenbach and C. Jung, Random tessellations: An overview of models, in *Stochastic Geometry: Percolation, Tesselations, Gaussian Fields and Point Processes*, edited by H. Biermé (Springer, Cham, Switzerland, 2025) pp. 35–80.

[32] M. P. do Carmo, *Differential Geometry of Curves and Surfaces* (Prentice-Hall, Sacramento, CA, USA, 1976).

[33] C. Villani, *Optimal Transport: Old and New* (Springer, Heidelberg, Germany, 2009).

[34] A. K. Chandra, P. Raghavan, W. L. Ruzzo, R. Smolensky, and P. Tiwari, Comput. Complex. **6**, 312 (1996).

[35] X. Wang, E. Pournaras, R. E. Kooij, and P. Van Mieghem, Eur. Phys. J. B **87**, 221 (2014).

[36] A. Ghosh, S. Boyd, and A. Saberi, SIAM Review **50**, 37 (2008).

[37] N. Masuda, M. A. Porter, and R. Lambiotte, Physics Reports **716–717**, 1 (2017).

[38] U. Kelathaya, R. B. Bapat, and M. P. Karantha, AKCE Int. J. Graphs Combin. **20**, 108 (2023).

[39] D. A. Levin, Y. Peres, and E. L. Wilmer, *Markov Chains and Mixing Times*, 2nd ed. (American Mathematical Society, Providence, RI, USA, 2017).

[40] A. C. Schwarze, J. Jiang, J. Wray, and M. A. Porter, arXiv preprint (2024), arXiv:2409.07498.

[41] O. Artime, M. Grassia, M. De Domenico, J. P. Gleeson, H. A. Makse, G. Mangioni, M. Perc, and F. Radicchi, Nat. Rev. Phys. **6**, 114 (2024).

[42] F. Ecevit and A. Boysal, Turk. J. Math. **49**, 18 (2025).

[43] L. Ye, Lin. Multilin. Alg. **59**, 645 (2011).

[44] K. Moody, M. Li, C. E. Maher, K. Lee, T. Horn, K. A. Newhall, R. Hurley, K. E. Daniels, and C. Rock (2025), under review.

[45] C.-C. Ni, Y.-Y. Lin, J. Gao, X. D. Gu, and E. Saucan, in *Proc. IEEE Conf. Comp. Comm. (INFOCOM) 2015* (2015) pp. 2758–2766.

[46] R. S. Sandhu, T. T. Georgiou, and A. R. Tannenbaum, Sci. Adv. **2**, e1501495 (2016).

[47] A. Gosztolai and A. Arnaudon, Nat. Comm. **12**, 4561 (2021).

[48] H. Cetinay, K. Devriendt, and P. Van Mieghem, Appl. Netw. Sci. **3**, 34 (2018).